APL Photonics

RESEARCH ARTICLE | JUNE 05 2025

Breaking boundaries of hybrid photodetector: A novel approach for high-speed TCSPC with minimal distortion

Special Collection: Single-photon detectors: new physical principles, circuits and applications

P. Daniele ; G. Fratta ; I. Labanca ; G. Acconcia ; I. Rech

APL Photonics 10, 060803 (2025)
https://doi.org/10.1063/5.0268205

APL Photonics ARTICLE pubs.aip.org/aip/app

Breaking boundaries of hybrid photodetector: A novel approach for high-speed TCSPC with minimal distortion

Cite as: APL Photon. 10, 060803 (2025); doi: 10.1063/5.0268205
Submitted: 28 February 2025 • Accepted: 22 May 2025 •
Published Online: 5 June 2025

P. Daniele,[a] G. Fratta, I. Labanca, G. Acconcia, and I. Rech

AFFILIATIONS

Dipartimento di Elettronica, Informazione e Bioingegneria, Politecnico di Milano, via Golgi 40, 20133 Milan, Italy

Note: This paper is part of the Special Topic on Single-Photon Detectors: New Physical Principles, Circuits and Applications.
[a]**Author to whom correspondence should be addressed:** piergiorgio.daniele@polimi.it

ABSTRACT

Time-Correlated Single-Photon Counting (TCSPC) enables the measurement of low-intensity optical signals with sub-picosecond timing resolution. Its performance has long been limited by pile-up distortion, which restricts acquisition rates to a small fraction (typically 5%) of the laser excitation rate. In this work, we break through these limitations in fluorescence measurements by harnessing the power of a hybrid photodetector and validating a novel, constraint-free methodology that removes pile-up distortion, enabling high precision in lifetime estimation. The mathematical framework underlying this method not only makes it possible to overcome the traditional distortion but also addresses previously unexplored error sources. For the first time, we present a real-time processing algorithm that compensates for hardware-induced distortions, achieving a comprehensive fluorescence histogram correction. Remarkably, with our approach, we achieve a count rate as high as 121% of the excitation rate, setting a new benchmark in TCSPC performance and representing a transformative leap forward in the capability of the technology to deliver high-speed and high-precision measurements.

I. INTRODUCTION

Time-Correlated Single-Photon Counting (TCSPC)[1–3] has gained significant relevance across a wide range of advanced scientific applications, including Fluorescence Lifetime Imaging Microscopy (FLIM),[4–7] single-molecule fluorescence analysis,[8–10] and Light Detection and Ranging (LiDAR) for both free-space and underwater environments.[11–13] Additionally, it plays a crucial role in quantum cryptography[14,15] and quantum optics.[16,17] In principle, the technique involves the periodic excitation of a sample through a high-rate pulsed laser source and the recording of the arrival times of the emitted photons. Photon detection relies on advanced single-photon detectors, such as Single Photon Avalanche Diodes (SPADs),[18–21] Hybrid Photodetectors (HPDs),[22,23] or Silicon Photomultipliers (SiPMs).[24,25] Timing circuits, including Time-to-Digital Converters (TDCs)[26] or Time-to-Amplitude Converters (TACs)[27] followed by Analog-to-Digital Converters (ADCs), convert the photon arrival times within the laser period into digital words. Finally, the collected data are processed by a computational unit, typically a Field-Programmable Gate Array (FPGA). Once a sufficient number of photon events have been recorded, the optical signal waveform emitted by the sample can be statistically reconstructed with high accuracy and sub-picosecond resolution.[28]

TCSPC hinges on the statistical accumulation of detected photons. The more the collected events, the lower the statistical noise, and the greater the accuracy and the reliability of the obtained results. However, the intrinsic statistical nature of the technique often requires extended acquisition times, limiting its efficiency and preventing it from reaching its full potential. Although it might seem intuitive to increase the excitation intensity to speed up the data acquisition, this approach is fundamentally limited by the dead time of the system, i.e., the period required by the detector and electronics to process an event. During this interval, subsequent photons cannot be registered, easily leading to the so-called *pile-up* distortion affecting the acquired TCSPC histograms. This unwanted distortion arises from three key phenomena: classic pile-up, detector dead time pile-up, and conversion dead time pile-up.[29,30] Classic pile-up occurs when the system cannot record multiple events within a single excitation period, whereas detector and conversion dead time pile-up result from the unresponsiveness of the detector and electronics while they process an event. To mitigate this phenomenon, the count rate in traditional TCSPC systems has historically been restricted to only a small fraction of the laser excitation rate, typically ranging from 1% to 5%.[1,29] This limitation ensures that the system processes each photon event accurately, reducing the likelihood of a photon impinging on the photodetector during the dead time, which, in turn, results in slower overall data acquisitions.

Although significant progress has been made in mitigating classic pile-up and electronic conversion pile-up—thanks to advances in multi-hit detection[31] and ultra-fast conversion electronics[27,32,33]—the finite dead time of detectors remains a key bottleneck for improving the acquisition speed in TCSPC-based applications. To address the challenge of improving system responsiveness, detectors with extremely low dead times, such as SPADs driven by Active Quenching Circuits (AQCs)[21,34,35] and HPDs,[23] have been developed. However, even these low-dead-time detectors can introduce distortions, especially when measuring short lifetimes under high-intensity illumination. Additionally, in the specific case of SPAD-based systems, low-dead-time operation can worsen issues such as afterpulsing, which further degrade data fidelity.[36] Recent innovations have sought to tackle pile-up distortion more effectively. In particular, multichannel systems have enabled multiple photon detections within a single excitation cycle,[37,38] while post-processing algorithms for pile-up correction have been developed—though they still require prior knowledge of the signal shape for optimal performance.[39,40] A pioneering approach to prevent pile-up distortion was proposed by Cominelli *et al.* in 2017.[41] It involves tuning the dead time of the detector to an integer multiple of the excitation period, thereby effectively eliminating distortion. While this approach has demonstrated operation at up to 65% of the laser excitation frequency,[42] it also imposes a limit on further dead time reductions.

In 2023, Rech *et al.*[43] presented a revolutionary theory that allows removing all constraints in TCSPC measurements, thus unlocking unprecedented speed potential. This approach was experimentally validated by Fratta *et al.* in Ref. 44, where it is demonstrated that the long-standing pile-up issue could be effectively resolved by incorporating system status information into the conventional TCSPC data histogram. This eliminates the need for prior knowledge of the signal shape and significantly overcomes the speed limitations of the technique. Notably, we achieved up to an average of 1.16 photons per period using a commercially available detection module. In this work, we validate the latter technique by leveraging a commercial HPD, which emerges as a highly promising solution, further extending the boundaries of the novel methodology. HPDs excel due to their unique combination of exceptionally short dead time (below one nanosecond), ultra-low dark counts, and negligible afterpulsing probability. The short dead time facilitates TCSPC measurements at extremely high photon count rates by allowing the use of high illumination power. Additionally, the extremely low dark count rate improves the signal-to-noise ratio while the negligible afterpulsing probability prevents any artifact potentially arising from correlated noise. These characteristics make the hybrid photodetector particularly well-suited for ultra-fast and high-precision measurements. While Hwang *et al.*[45] harnessed the number-resolving capabilities of HPDs to achieve a single-photon counting rate of 29% of the laser excitation frequency, our approach surpasses this benchmark by integrating the pile-up correction algorithm, enabling an unprecedented count rate exceeding 120% of the excitation frequency, with the throughput of the timing system acting as the limiting factor for further increases. This unprecedented photon count rate marks a significant advancement for applications characterized by intense light signals, which are typically limited by distortion effects in TCSPC. The goal is to demonstrate that TCSPC is not restricted to low-count-rate scenarios but can also be a powerful tool for ultra-fast, high-intensity applications, ensuring both high resolution and efficiency.

This paper is structured as follows: Sec. II details the methodology and experimental setup underpinning our measurements. In Sec. III, we identify and address non-idealities in the output voltage signal of the detector, revealing their role in generating histogram distortions beyond traditional pile-up effects. For the first time, we introduce a post-processing correction algorithm capable of compensating for these hardware-induced distortions, delivering comprehensive and precise histogram correction. This paper concludes by synthesizing the key findings, emphasizing the broader impact of our contributions and outlining promising directions for future research.

II. PILE-UP DISTORTION: ANALYSIS AND CORRECTION

A. Methodology

The pile-up phenomenon has been rigorously explored in the previous studies by Cominelli *et al.* in Ref. 41 and further examined by Rech *et al.* in Ref. 43. When the photon arrival rate exceeds the capacity of the detection system, the finite dead time, T_{dead}, causes subsequent photons to be missed, leading to counting losses and significant distortion. By leveraging the advanced capabilities of the HPD, the proposed technique ensures that missed photon events are accurately reconstructed, even when the excitation rate exceeds the typical pile-up threshold. As outlined in Refs. 43 and 44, we define $r_{rec}(t)$ as the distribution of recorded photons, given by the product of the average number of photons per laser period, $\mathscr{P}$, and the probability density function $P_{rec}(t)$, which describes the likelihood of a photon being recorded at time t. In contrast, $r_{imp}(t)$ denotes the distribution of photons impinging on the photodetector. Thus, $r_{rec}(t)$ reflects the measured response of the system, affected by pile-up distortion, while $r_{imp}(t)$ represents the actual photon distribution at the detector, as sketched in Fig. 1, for a single exponential decay.

The relationship between $r_{imp}(t)$ and $r_{rec}(t)$ is given by the following equation:

$$r_{imp}(t) = \frac{r_{rec}(t)}{\alpha(t)}, \quad (1)$$

where function $\alpha(t)$ represents the probability function that tracks the activity of the system during each laser period throughout the measurement process. In other words, $\alpha(t)$ indicates the probability that the system is capable of detecting photons at a given time t, taking into account the effects of the dead time of the system.

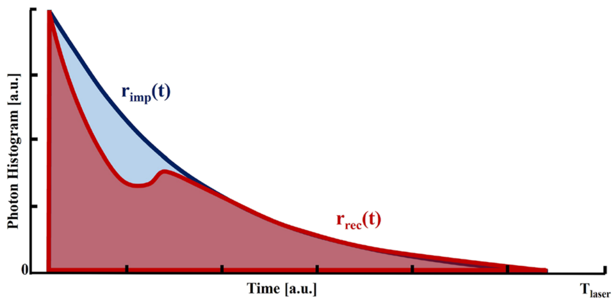

FIG. 1. Sketch of a TCSPC data histogram affected by distortion at high-count rates. The red curve represents the distribution of recorded photons, $r_{rec}(t)$, while the blue curve represents the distribution of photons impinging on the photodetector, $r_{imp}(t)$.

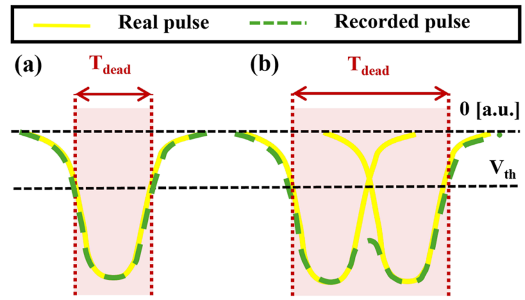

FIG. 2. (a) Photon losses during T_{dead} of each detected event. (b) Overlapping photons fail to surpass the detection threshold.

Specifically, $\alpha(t)$ serves as a weighting factor for photons detected at time t, accounting for the correction due to the dead time triggered by each photon event occurring within $t - T_{dead}$.

At this point, we can briefly recall the key theoretical concept behind the run-time reconstruction of $\alpha(t)$, focusing on its physical significance. This process involves dividing the laser period into discrete time bins, each with a width corresponding to the timing resolution of the measurement system. At each laser period when the system is active, the count for the respective time bins is incremented by 1. If, however, the detector enters a dead time during a given interval, the count for those bins remains unchanged (i.e., it is not incremented). This process is repeated for each excitation cycle, accumulating data that reflect the timing behavior of the detector over time. Afterward, the function is normalized by the total number of periods for which the measurement is conducted. This normalization ensures that $\alpha(t)$ remains within the range $(0, 1)$ and that its total area equals 1, thereby fulfilling the requirements of a valid detection probability.

In this framework, it is essential to define the concept of dead time and its specific characterization in the context of HPD-based TCSPC measurements. When a photon is detected, the timing output signal of the HPD—a negative voltage pulse with a fast rise time—must be acquired by an acquisition system, which can use either a Constant Fraction Discriminator (CFD) or a comparator with a fixed voltage threshold. In our setup, we use the latter approach, which will be discussed in detail in Sec. II B.

We define the HPD dead time as the time difference between the time instant at which the falling edge crosses the comparator threshold (marking the photon arrival time) and the time instant corresponding to the rising edge crossing the comparator threshold again, indicating that the system is ready to detect another event. Indeed, in this time interval, the electronics cannot register any further event. A typical scenario with a single event is sketched in Fig. 2(a). Nevertheless, another possible scenario must also be considered: when photon emissions occur in rapid succession—specifically when the time interval between events is shorter than the width of the output voltage pulse—photon overlap occurs, as shown in Fig. 2(b). The overlapping photons fail to surpass the chosen detection threshold, leading to the failure to detect the combined signal. Consequently, merged pulses cannot be distinguished by the TCSPC electronics, resulting not only in information loss but also in a variation of the detector effective dead time. Traditional correction methods often rely on prior knowledge of the signal shape and assume a fixed T_{dead},[40] but these approaches do not address photon overlap as they mainly focus on approximation-based reconstruction. Although Meyer *et al.* introduced a post-processing statistical pile-up correction algorithm,[46] our novel method effectively compensates for this additional distortion by exploiting $\alpha(t)$, which accounts for the effective T_{dead} during which the system is unable to detect photons.

B. Experimental setup

The experimental setup is depicted in Fig. 3. The illumination source is a high-end picosecond diode laser driver (PicoQuant GmbH, Taiko PDL M1) connected to an LDH-I series pulsed diode laser cuboid head. The laser, operating at an excitation frequency of 20 MHz, features an emission wavelength of 470 nm and a pulse full-width at half-maximum (FWHM) of 80 ps. The laser output is coupled to a fiber delivering the light to a diluted solution of Coumarin-6 in ethanol, featuring a time constant approximately equal to 3.2 ns. The fluorescence signal produced by the sample passes through a circular reflective neutral density filter (by Thorlabs), allowing us to select various attenuation factors. Finally, the light is directed to a commercial detection module incorporating a hybrid photodetector (PicoQuant, PMA Hybrid Series), employing a fast hybrid photomultiplier tube (Hamamatsu, R10467). The

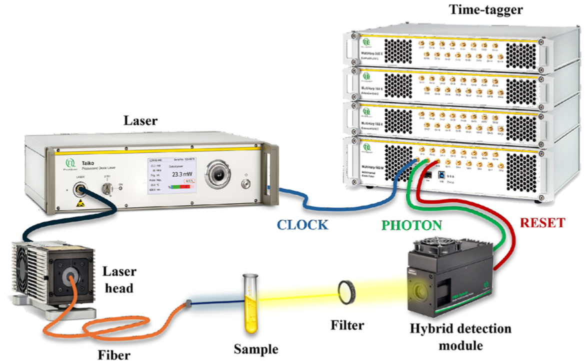

FIG. 3. Experimental setup for the validation of the proposed pile-up correction methodology.

timing output of the detection module is a short negative voltage pulse with a fast rise time and a nominal amplitude of ~−200 mV. As explained in Sec. II A, for each detected photon, the signal must be acquired at both the falling and rising edges. The dead time, defined as the temporal difference between these edges, is ~1.2 ns. Edge detection can be performed using either a CFD or a comparator. While a CFD improves timing accuracy by adjusting the threshold crossing time based on the amplitude of the signal, its implementation to measure the time difference between edges would introduce additional system complexity. Given that a commercial multichannel event timer (PicoQuant GmbH, MultiHarp 160M) operating in time-tagging mode is already required for event timestamping, we assessed the timing performance using a direct detection approach with the internal comparators of the event timer. By setting the comparator threshold voltage to V_{th} = −50 mV and synchronizing with the reference clock of the laser (CLOCK), the Instrument Response Function (IRF) of the system, which incorporates contributions from both the laser (80 ps FWHM) and the event timer (105 ps FWHM), remains negligible compared to the intensity profile of the light emitted by the sample. Consequently, the direct

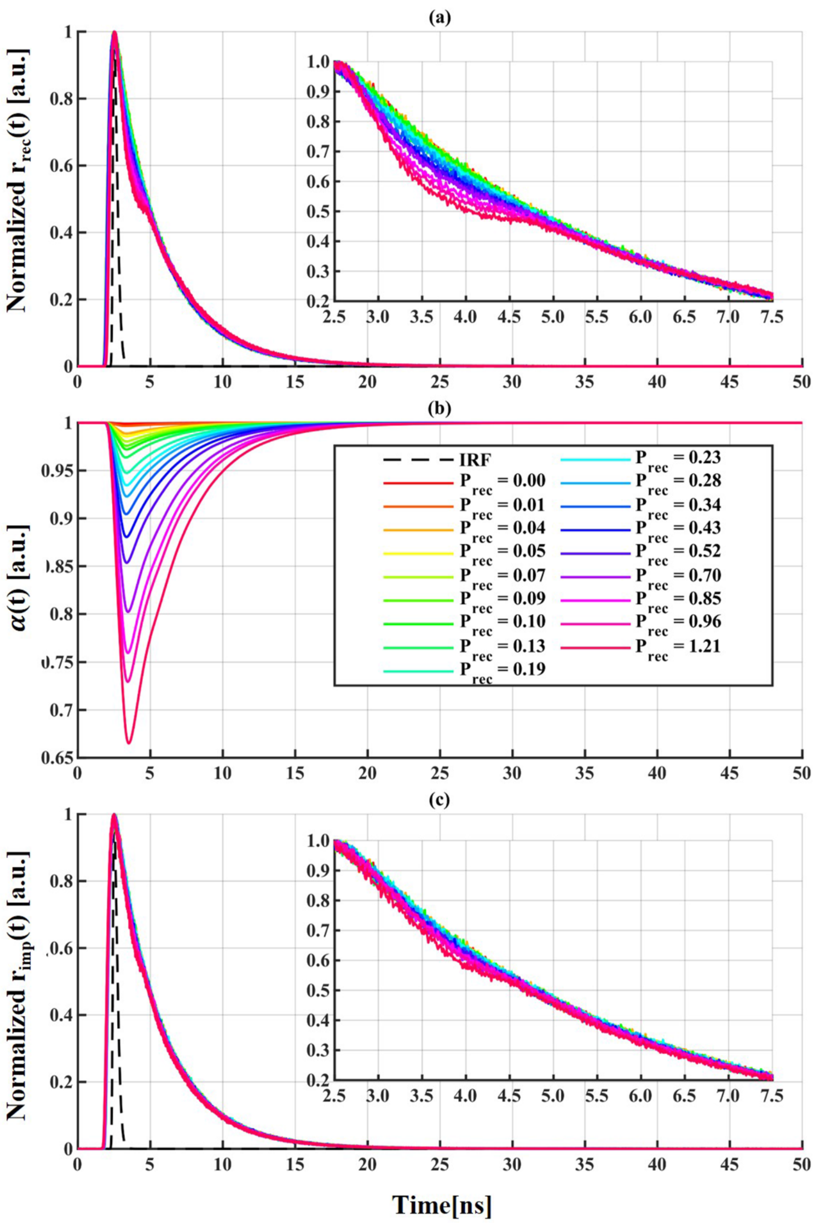

FIG. 4. Application of the pile-up correction algorithm to the fluorescence exponential decay histograms for various $P_{rec}(t)$ values. (a) Acquired histograms showing the pile-up distortion. (b) Probability $\alpha(t)$ of the detector to be active. (c) Corrected histograms after the application of Eq. (1).

approach using the internal comparators of the event timer with a fixed threshold of $V_{th} = -50$ mV was adopted.

Two channels of the event timer are used: one channel detects the falling edge (PHOTON), while the other captures the rising edge (RESET). The measurements were performed using a fixed laser power of 1.59 mW (10% of the maximum power provided by the laser) and using different filters to progressively decrease the attenuation factor. In this way, the average number of photons impinging on the photodetector within the signal period can be varied, reaching values that are well above the historical limits of TCSPC.

C. Results and discussion

The experimental results are presented in Fig. 4, demonstrating the effectiveness of the distortion correction methodology. Figure 4(a) shows the acquired TCSPC data histograms, normalized to the peak, at various recorded power levels, P_{rec}. As the excitation power increases, the photon count rate rises, pushing the system beyond the pile-up-safe regime and amplifying the resulting distortion. The measured behavior is consistent with the expected performance of classic TCSPC systems under high-excitation conditions. In Fig. 4(b), the probability function $\alpha(t)$ is shown for all values of $P_{rec}(t)$. This function is crucial for correcting the recorded histograms as it ensures the accurate accounting of photon detection events that are lost due to the dead time of the system. Finally, Fig. 4(c) presents the corrected data histograms, obtained by applying Eq. (1). This correction effectively compensates for distortions caused by both the dead time losses and the photon overlaps, even at very high power levels. By leveraging $\alpha(t)$, we recover the lost photon information, reproducing the corrected, distortion-free histograms, thus greatly enhancing the accuracy and reliability of TCSPC measurements.

Figure 5 shows the estimated lifetimes of the distorted (in red) and the corrected (in blue) histograms as $P_{rec}(t)$ increases. The lifetime values were determined by fitting the fluorescence decay curves using the same methodology described in Ref. 44. As $P_{rec}(t)$ increases, the distortion becomes more pronounced, leading to a progressive overestimation of the lifetime. However, after applying the proposed correction algorithm, the estimated lifetime stabilizes around 3.2 ns, with an error between −0.13% and +0.98%. Specifically, the percentage error E[%] is calculated using the following equation:

$$E[\%] = \frac{\tau_{high-rate} - \tau_{low-rate}}{\tau_{low-rate}} \cdot 100. \quad (2)$$

This analysis demonstrates the effectiveness of the novel, constraint-free pile-up correction technique, which enables fluorescence measurements with a HPD at 121% of the excitation rate for the first time. However, a critical issue remains: as shown in Fig. 4(c), a residual distortion is still evident in the high-rate curves. To quantitatively assess the distortion, an error deviation analysis is performed on each temporal bin by comparing histograms acquired at various $H_{low\text{-}rate}(t)$ values against a reference histogram measured at low count rates. The percentage error $E(t)[\%]$ at each time instant t calculated for each comparison and reported in Fig. 6 is given by the following expression:

$$E(t)[\%] = \frac{H_{high-rate}(t) - H_{low-rate}(t)}{H_{low-rate}(t)} \cdot 100, \quad (3)$$

where $H_{high\text{-}rate}(t)$ refers to the corresponding measured distorted histogram value acquired at a count rate exceeding the pile-up limit and $H_{low\text{-}rate}(t)$ is the corresponding value from the low-count-rate reference. The measured peak-to-peak error increases with increasing $P_{rec}(t)$. This behavior highlights the need for further investigation, which is addressed in Sec. III.

III. HARDWARE DISTORTION: ANALYSIS AND CORRECTION

A. Methodology

The correction technique described in Sec. II effectively eliminates pile-up distortion by employing information extracted from the acquired data, particularly the timing of photon arrivals and the completion of the corresponding processing cycle. The mathematical framework underlying this method not only makes it possible to overcome the traditional distortion but also reveals previously unexplored sources of error. Indeed, as shown in Figs. 4(c) and 6, it is worth observing that the effectiveness of the correction decreases

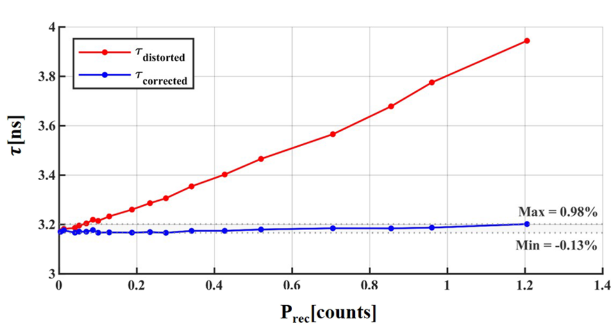

FIG. 5. Trend of the estimated lifetimes of the distorted histograms (red curve) and the corrected histograms (blue curve) as $P_{rec}(t)$ increases. The blue curve also includes the maximum and minimum committed error in the lifetime estimation.

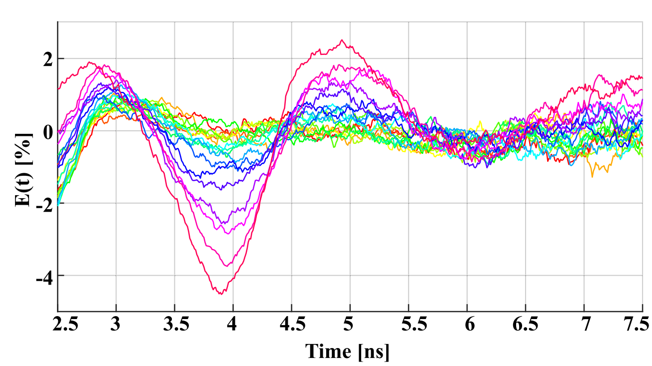

FIG. 6. Error deviation analysis between histograms acquired at increasing $P_{rec}(t)$ values and the low-count-rate reference. The percentage error E(t) is computed for each temporal bin according to Eq. (3). A growing peak-to-peak distortion is observed with increasing $P_{rec}(t)$.

for high-rate curves. Specifically, in the 5 ns window following the fluorescence peak, starting just after T_{dead}, an anomalous deviation from the expected exponential decay curve becomes evident. In TCSPC-based fluorescence measurements, where photon arrival times follow an inhomogeneous Poisson distribution during each excitation cycle, increasing $P_{rec}(t)$ not only increases the average number of detected photons per period but also increases the likelihood of photons arriving close to each other. In our case, two close photons can lead to two primary effects: first, photons may merge into a single event if they fail to exceed the set detection threshold [as reported in Sec. II and illustrated in Fig. 2(b)], and second, timing data can be corrupted by ringing disturbances in the output voltage signal of the detector module, if present. While the photon merging effect is effectively corrected by the method described in Sec. II, which accounts for the effective dead time of the system after each photon event within the function $\alpha(t)$ and applies it to correct the TCSPC data histogram, timing errors induced by voltage ringing remain unaddressed. To mitigate this issue, the present analysis introduces a novel post-processing correction algorithm. This approach ensures accurate lifetime estimations even in high-count rate scenarios.

Figure 7 illustrates the envelope of the HPD timing output signal, with the trigger set on the falling edge at an appropriate threshold level. The signal is displayed with infinite persistence on a 1-GHz-bandwidth oscilloscope (Tektronix, 3 Series MDO), providing a detailed view of the temporal response of the detector over time. This high-resolution visualization highlights the precise characteristics of the timing output signal, offering a clear understanding of its behavior. Notably, attention should be paid to the irregular voltage ringing observed during the first 5 ns after the detection point of the photon pulse. Once a photon is detected and its corresponding voltage ringing is triggered, any subsequent photon arriving within the disturbed window will be affected by the lingering effects of the previous signal. This interference results in corrupted timing for the second event. Such a phenomenon is illustrated in Fig. 8, which shows two consecutive detected events.

The second photon starts at a shifted voltage level, causing it to be sampled at an incorrect time, which introduces timing inaccuracies and leads to further distortion in the recorded histogram. It is worth saying that temporal inaccuracies in signal discrimination

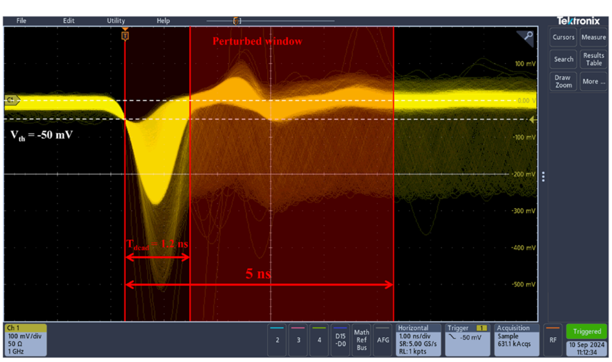

FIG. 7. Envelope of the timing output signal from the HPD, displayed with infinite persistence and triggered on the falling edge at $V_{th} = -50$ mV, captured using a 1-GHz-bandwidth oscilloscope (Tektronix, 3 Series MDO).

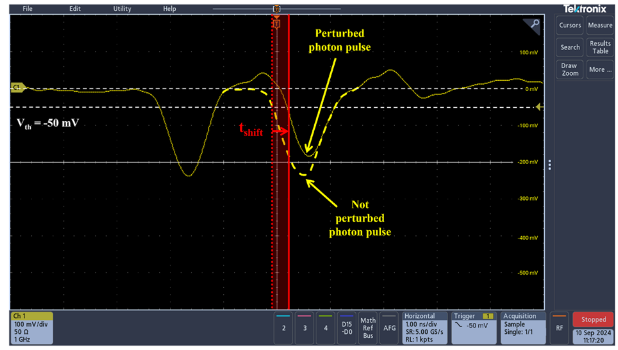

FIG. 8. Example of two closely spaced photon events. The second photon, within the perturbed 5 ns window, begins at a shifted voltage level, causing it to be sampled at an incorrect time.

are typically addressed using a CFD. For signals with varying amplitude, the key advantage of a CFD is its ability to record timestamps at a fixed fraction of the peak's height, ensuring precise timing measurements. The CFD works by splitting the incoming pulse into two components: the lower portion is inverted, and the higher portion is delayed. These components are then recombined. The point where they combine, known as the zero-crossing point, remains unaffected by the amplitude of the signal. However, in our case, the inaccuracy arises not from amplitude variation but from a signal offset, as explained earlier. We can analyze the impact of the CFD with an offset on the signal using the following equation:

$$V_{CFD}(t) = (V_{in}(t-\tau) + V_{off}) - A(V_{in}(t) + V_{off}), \quad (4)$$

where $V_{CFD}(t)$ is the CFD output voltage signal, $V_{in}(t)$ is the input voltage signal, V_{off} is the voltage offset affecting $V_{in}(t)$, and A defines the point on the waveform where the comparison with the delayed version of the signal occurs. For signals with fast rising edges, such as the timing output from the HPD, typical values of A range between 0.2 and 0.4. By solving Eq. (4), we obtain

$$V_{CFD}(t) = V_{in}(t-\tau) - AV_{in}(t) + (1-A)V_{off}. \quad (5)$$

Figure 9 provides a graphical representation of the result obtained in (5). The offset introduces an additional term that affects the operation of the CFD, shifting the zero-crossing point and thereby introducing an error in the timing measurement. Therefore, to correct the distortion introduced by the HPD timing signal, we propose an alternative approach based on its experimental characterization. A key aspect of this approach is that it relies solely on the characterization of the timing output signal of the detector, independent of other measurement variables. A key requirement of this analysis is to establish a clear correlation between the true arrival time, t_{real}, and the measured time of the in-window photon, t_{meas}. Section III B details the experimental setup used to determine this correlation in terms of the timing shift between t_{real} and t_{meas} along with the corresponding correction algorithm.

B. Experimental setup

The experimental setup used for analyzing hardware distortion is depicted in Fig. 10. Two synchronized laser sources are employed,

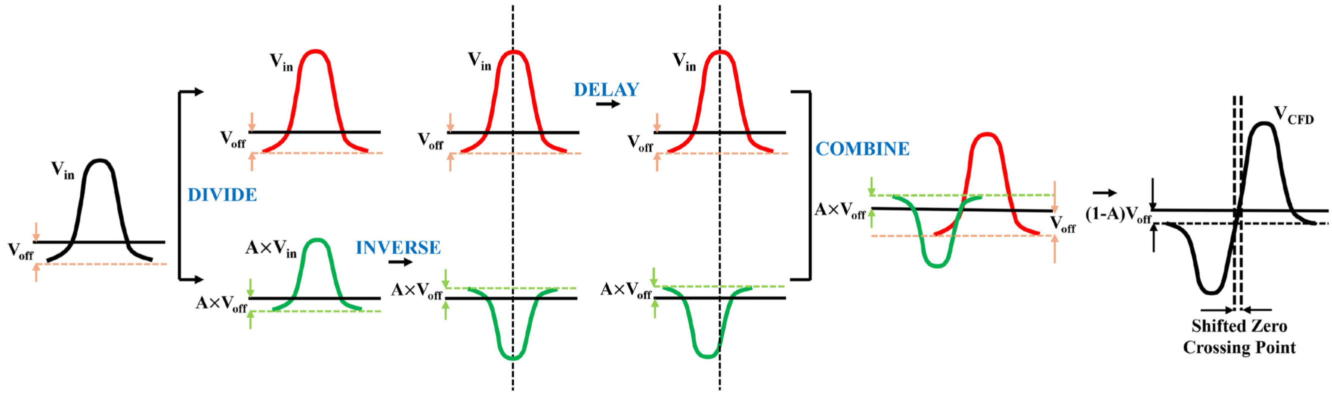

FIG. 9. Graphical representation of the result obtained in (5). The presence of an offset introduces an additional term that alters the operation of the CFD, shifting the zero-crossing point and resulting in a timing error.

with a controlled and progressively decreasing delay introduced between them. The first laser (A.L.S GmbH, Advanced Laser Diode Systems) operates at an emission wavelength of 850 nm with a pulse FWHM of 35 ps. The second laser (PicoQuant GmbH, Taiko PDL M1), previously utilized in the setup in Sec. II, emits at 470 nm with a pulse FWHM of 80 ps. The repetition frequency of both lasers is set by a fast rise-time pulse generator (Active Technologies, Pulse Rider PG-1074), which provides an external trigger signal at 1 MHz. The pulse generator produces two delayed square waves with a pulse width of 500 ns and a period of 1 μs. One wave (SYNC 2) is delayed with respect to the other (SYNC 1), ensuring synchronization while introducing a progressively decreasing delay between the two lasers, starting from 5 ns. This configuration enables the simulation of two distinct, closely spaced photon events within the perturbed window. The output signal from the detector (PHOTON) is fed to one channel of the event timer (PicoQuant GmbH, MultiHarp 160M), which is synchronized to the first laser through the pulse generator (CLOCK).

C. Results and discussion

The photon events from the first laser (Laser 1 in Fig. 10) consistently appear at a fixed position within the laser period, providing a reliable temporal reference. In contrast, the photon events from the second laser (Laser 2 in Fig. 10)—those occurring within the perturbed window caused by the first laser events—exhibit a mismatch, t_{shift}, between the recorded arrival times, t_{meas}, and the actual temporal delay set between the two light sources, t_{real}. This discrepancy arises because the event timer relies on a fixed voltage threshold for photon detection. Consequently, pulses starting from a positive ringing level are detected later than their true arrival time (as shown in the specific example displayed in Fig. 8), while those starting from a negative ringing level are detected earlier. To determine t_{shift} as a function of t_{real}, we analyze the position of the peak in the reconstructed histogram corresponding to the second laser, considering only instances where a preceding photon event from the first laser is present. For example, as illustrated by the red curve in Fig. 11, when the actual delay is t_{real} = 2 ns, the corresponding timing shift is t_{shift} = 110 ps, resulting in the event measured at t_{meas} = 2.11 ns. Starting from the measured timing shift as a function of the true set delay, $t_{shift}(t_{real})$, we can establish the relationship between t_{meas} and t_{real} using the following equation:

$$t_{meas} = t_{real} + t_{shift}(t_{real}). \tag{6}$$

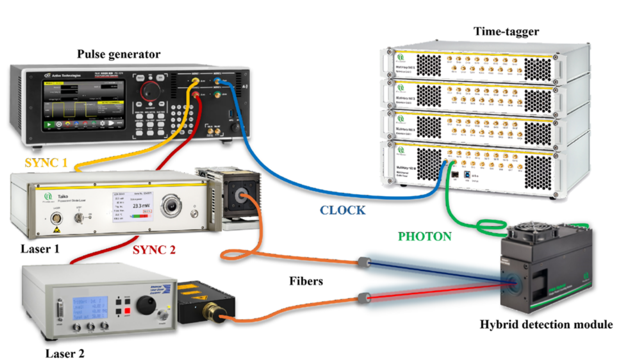

FIG. 10. Experimental setup for obtaining $t_{shift}(t_{real})$ for the proposed correction algorithm addressing hardware-induced distortions.

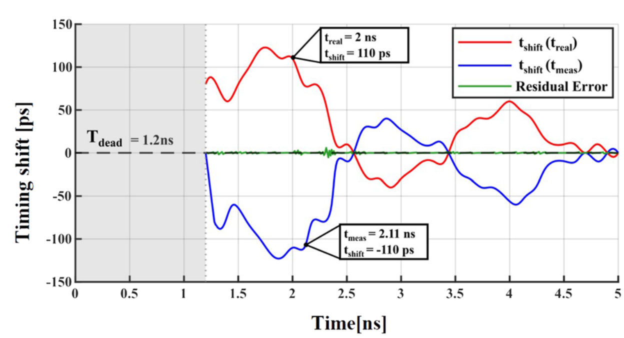

FIG. 11. Representation of the timing shift as a function of the set delay between the two laser sources (red curve), along with the timing shift that must be removed as a function of the measured delay (blue curve). The green curve represents the residual error in the timing shift determined by the finite timing resolution of the system.

Thus, t_{shift} can be expressed in terms of t_{meas}. When a photon is detected, the time of arrival of a subsequent event falling within 5 ns from the end of the first photon dead time must be corrected, substituting its t_{meas} with the corresponding computed t_{real}. Referring to the previous example, when the measured photon arrival time of the second photon is t_{meas} = 2.11 ns, the corresponding t_{shift} = −110 ps can be applied to recover the true photon arrival time, t_{real} = 2 ns. This inverse relationship is visually represented by the blue curve in Fig. 11. Furthermore, the green curve illustrates the residual error in the timing shift, which is determined by the finite timing resolution of 10 ps, which highlights the precision of the correction algorithm within the inherent limitations of the system.

To further evaluate the effectiveness of the proposed correction method, a custom MATLAB-based simulator was employed to replicate the hardware-induced disturbances under identical experimental conditions, specifically at 1.21 photons per excitation period. The experimentally retrieved $t_{shift}(t_{real})$ values were applied to each photon event simulated within the perturbed window, following the fluorescence peak. Figure 12(a) presents a comparison between the high-rate histogram, both experimentally measured (red curve) and simulated (blue curve), including hardware-induced distortions, and after the application of the pile-up correction methodology, compared with the reference histogram obtained under low-rate conditions. The excellent alignment between the experimental and simulated results validates the accuracy and reliability of the simulation. Additionally, Fig. 12(b) illustrates the error deviation between the high-rate histograms (both measured and simulated) and the low-rate reference one. As illustrated in Fig. 12(b), the measured peak-to-peak error is 7.12%.

Figure 12(c) presents the corrected histograms obtained after sequentially applying the described correction algorithm followed by the pile-up correction methodology to both the simulated and experimentally measured distorted histograms. This figure compares the high-rate histograms with the low-rate reference, clearly

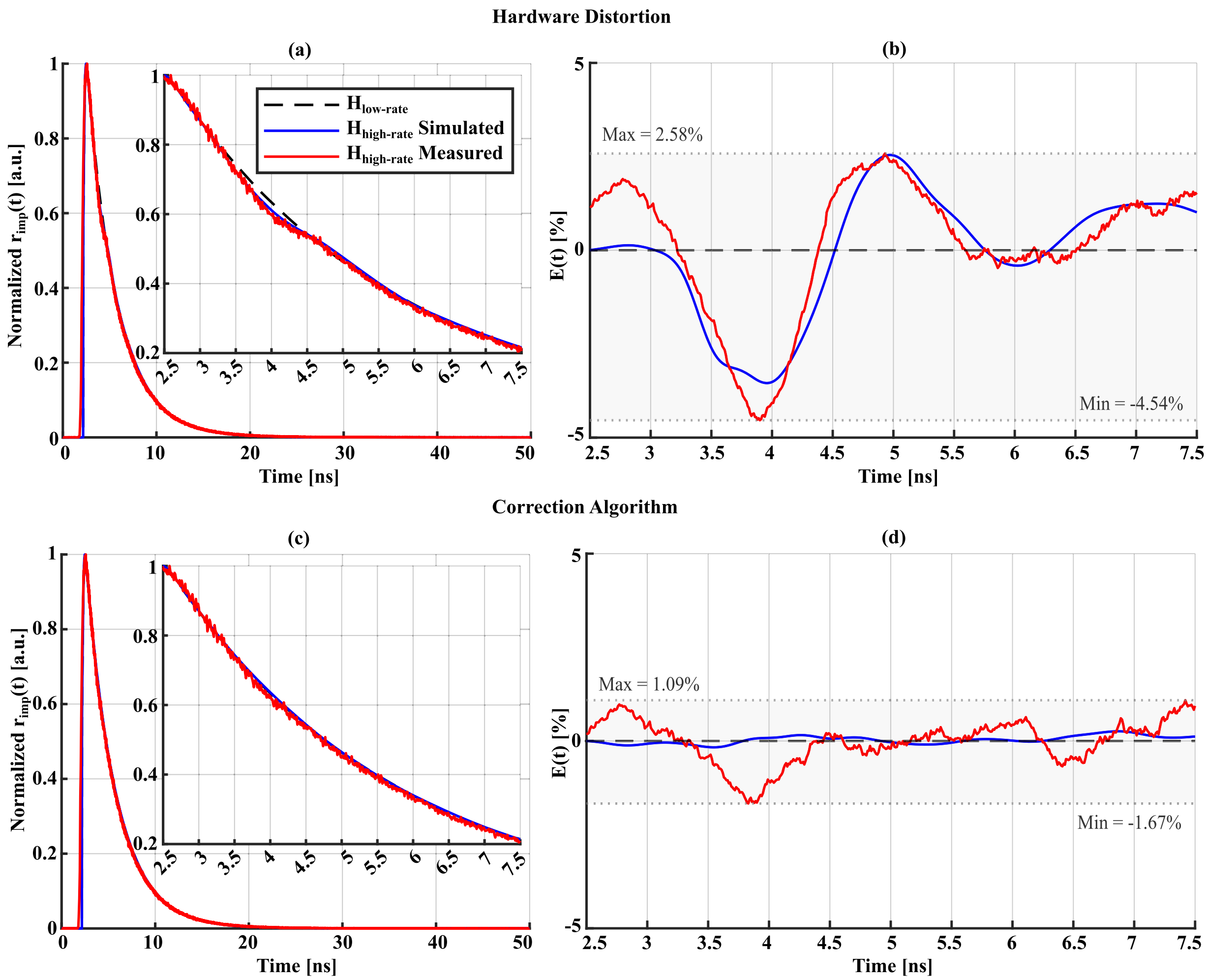

FIG. 12. TCSPC histograms and error deviation plots under different correction conditions. (a) and (c) show the histograms obtained from both experimental and simulated data after applying only the pile-up correction and both pile-up and hardware corrections, respectively. (b) and (d) display the corresponding error deviation plots under the same conditions.

demonstrating the effectiveness of the dual-correction approach. The pile-up correction effectively compensates for the photon overlap distortions, while the hardware correction addresses the timing inaccuracies introduced by the output voltage ringing. To quantitatively assess the performance of these corrections, Fig. 12(d) presents the percentage error deviation between the corrected high-rate histogram and the low-rate reference one, according to Eq. (3).

The peak-to-peak error is reduced to just 2.76%. This substantial reduction demonstrates the robustness of the proposed correction method, effectively compensating for any kind of distortions even under high photon flux conditions.

IV. CONCLUSION

In this work, we have successfully addressed the long-standing challenge of pile-up distortion at high rates in TCSPC. By leveraging a HPD and exploiting a robust mathematical framework, we have not only overcome the traditional limitations but also accounted for previously unrecognized sources of error. Our proposed post-processing algorithm effectively corrects both the pile-up distortion and hardware-induced artifacts, enabling ultra-precise fluorescence lifetime estimation. The results demonstrate an unprecedented ability to achieve count rates exceeding 120% of the excitation rate with a lifetime estimation error as low as 1.11% peak-to-peak and an extremely high fidelity of the reconstructed waveform, setting a new benchmark in TCSPC performance. This advancement marks a significant step forward, offering the potential for more accurate, high-speed measurements in a variety of scientific applications and opening up new possibilities for the study of ultra-fast processes in fluorescence and beyond.

ACKNOWLEDGMENTS

This work was supported by Ministero dell'Università e della Ricerca (PRIN2022, Proactive) and the European Research Council (HÈRMES, Grant No. 101116943).

AUTHOR DECLARATIONS

Conflict of Interest

The authors have no conflicts to disclose.

Author Contributions

P. Daniele: Data curation (lead); Investigation (lead); Writing – original draft (lead); Writing – review & editing (lead). **G. Fratta**: Data curation (equal); Investigation (equal). **I. Labanca**: Data curation (equal); Investigation (equal); Methodology (equal); Supervision (equal). **G. Acconcia**: Conceptualization (equal); Investigation (equal); Methodology (equal); Supervision (equal). **I. Rech**: Conceptualization (equal); Investigation (equal); Methodology (equal); Supervision (equal).

DATA AVAILABILITY

The data that support the findings of this study are available from the corresponding author upon reasonable request.

REFERENCES

[1] W. Becker, *Advanced Time-Correlated Single Photon Counting Applications* (Springer, 2015), Vol. 111.

[2] L. M. Hirvonen and K. Suhling, "Wide-field TCSPC: Methods and applications," Meas. Sci. Technol. **28**, 012003 (2016).

[3] W. Becker, A. Bergmann, and C. Biskup, "Multispectral fluorescence lifetime imaging by TCSPC," Microsc. Res. Tech. **70**, 403–409 (2007).

[4] K. Suhling, L. M. Hirvonen, J. A. Levitt, P.-H. Chung, C. Tregidgo, A. Le Marois, D. A. Rusakov, K. Zheng, S. Ameer-Beg, S. Poland *et al.*, "Fluorescence lifetime imaging (FLIM): Basic concepts and some recent developments," Med. Photonics **27**, 3–40 (2015).

[5] X. Liu, D. Lin, W. Becker, J. Niu, B. Yu, L. Liu, and J. Qu, "Fast fluorescence lifetime imaging techniques: A review on challenge and development," J. Innovative Opt. Health Sci. **12**, 1930003 (2019).

[6] R. Datta, T. M. Heaster, J. T. Sharick, A. A. Gillette, and M. C. Skala, "Fluorescence lifetime imaging microscopy: Fundamentals and advances in instrumentation, analysis, and applications," J. Biomed. Opt. **25**, 071203 (2020).

[7] J. Qu, L. Liu, D. Lin, and T. Y. Ohulchanskyy, "Fluorescence lifetime imaging microscopy and its biomedical applications," in *Asia Communications and Photonics Conference* (Optica Publishing Group, 2021), p. M5G-1.

[8] I. Rech, G. Luo, M. Ghioni, H. Yang, X. S. Xie, and S. Cova, "Photon-timing detector module for single-molecule spectroscopy with 60-ps resolution," IEEE J. Sel. Top. Quantum Electron. **10**, 788–795 (2004).

[9] B. Schuler and W. A. Eaton, "Protein folding studied by single-molecule fret," Curr. Opin. Struct. Biol. **18**, 16–26 (2008).

[10] E. Lerner, T. Cordes, A. Ingargiola, Y. Alhadid, S. Chung, X. Michalet, and S. Weiss, "Toward dynamic structural biology: Two decades of single-molecule Förster resonance energy transfer," Science **359**, eaan1133 (2018).

[11] A. McCarthy, R. J. Collins, N. J. Krichel, V. Fernández, A. M. Wallace, and G. S. Buller, "Long-range time-of-flight scanning sensor based on high-speed time-correlated single-photon counting," Appl. Opt. **48**, 6241–6251 (2009).

[12] A. Maccarone, A. McCarthy, X. Ren, R. E. Warburton, A. M. Wallace, J. Moffat, Y. Petillot, and G. S. Buller, "Underwater depth imaging using time-correlated single-photon counting," Opt. Express **23**, 33911–33926 (2015).

[13] R. Tobin, A. Halimi, A. McCarthy, P. J. Soan, and G. S. Buller, "Robust real-time 3D imaging of moving scenes through atmospheric obscurant using single-photon lidar," Sci. Rep. **11**, 11236 (2021).

[14] R. Terhaar, J. Rödiger, M. Häußler, M. Wahl, H. Gehring, M. A. Wolff, F. Beutel, W. Hartmann, N. Walter, J. Hanke *et al.*, "Ultrafast quantum key distribution using fully parallelized quantum channels," Opt. Express **31**, 2675–2688 (2023).

[15] J. Yang, Z. Jiang, F. Benthin, J. Hanel, T. Fandrich, R. Joos, S. Bauer, S. Kolatschek, A. Hreibi, E. P. Rugeramigabo *et al.*, "High-rate intercity quantum key distribution with a semiconductor single-photon source," Light: Sci. Appl. **13**, 150 (2024).

[16] A. Korneev, Y. Vachtomin, O. Minaeva, A. Divochiy, K. Smirnov, O. Okunev, G. Gol'Tsman, C. Zinoni, N. Chauvin, L. Balet *et al.*, "Single-photon detection system for quantum optics applications," IEEE J. Sel. Top. Quantum Electron. **13**, 944–951 (2007).

[17] R. Tenne, U. Rossman, B. Rephael, Y. Israel, A. Krupinski-Ptaszek, R. Lapkiewicz, Y. Silberberg, and D. Oron, "Super-resolution enhancement by quantum image scanning microscopy," Nat. Photonics **13**, 116–122 (2019).

[18] A. Gulinatti, I. Rech, P. Maccagnani, M. Ghioni, and S. Cova, "Large-area avalanche diodes for picosecond time-correlated photon counting," in *Proceedings of 35th European Solid-State Device Research Conference, 2005. ESSDERC 2005* (IEEE, 2005), pp. 355–358.

[19] F. Villa, B. Markovic, S. Bellisai, D. Bronzi, A. Tosi, F. Zappa, S. Tisa, D. Durini, S. Weyers, U. Paschen, and W. Brockherde, "SPAD smart pixel for time-of-flight and time-correlated single-photon counting measurements," IEEE Photonics J. **4**, 795–804 (2012).

[20] T. Al Abbas, N. Dutton, O. Almer, S. Pellegrini, Y. Henrion, and R. Henderson, "Backside illuminated SPAD image sensor with 7.83 μm pitch in 3D-stacked CMOS technology," in *2016 IEEE International Electron Devices Meeting (IEDM)* (IEEE, 2016), p. 8.

[21] F. Gramuglia, M.-L. Wu, C. Bruschini, M.-J. Lee, and E. Charbon, "A low-noise CMOS SPAD pixel with 12.1 Ps SPTR and 3 ns dead time," IEEE J. Sel. Top. Quantum Electron. **28**, 3800809 (2022).

[22] X. Michalet, A. Cheng, J. Antelman, M. Suyama, K. Arisaka, and S. Weiss, "Hybrid photodetector for single-molecule spectroscopy and microscopy," Proc. SPIE **6862**, 68620F (2008).

[23] PicoQuant, "PMA hybrid series," https://www.picoquant.com/products/category/photon-counting-detectors/pma-hybrid-series-hybrid-photomultiplier-detector-assembly.

[24] E. Martinenghi, L. Di Sieno, D. Contini, M. Sanzaro, A. Pifferi, and A. Dalla Mora, "Time-resolved single-photon detection module based on silicon photomultiplier: A novel building block for time-correlated measurement systems," Rev. Sci. Instrum. **87**, 073101 (2016).

[25] M. Caccia, L. Nardo, R. Santoro, and D. Schaffhauser, "Silicon photomultipliers and SPAD imagers in biophotonics: Advances and perspectives," Nucl. Instrum. Methods Phys. Res., Sect. A **926**, 101–117 (2019).

[26] N. A. Dutton, S. Gnecchi, L. Parmesan, A. J. Holmes, B. Rae, L. A. Grant, and R. K. Henderson, "11.5 a time-correlated single-photon-counting sensor with 14GS/S histogramming time-to-digital converter," in *2015 IEEE International Solid-State Circuits Conference-(ISSCC) Digest of Technical Papers* (IEEE, 2015), pp. 1–3.

[27] G. Acconcia, F. Malanga, S. Farina, M. Ghioni, and I. Rech, "A 1.9 ps-rms precision time-to-amplitude converter with 782 fs LSB and 0.79%-rms DNL," IEEE Trans. Instrum. Meas. **72**, 2003711 (2023).

[28] M. Köllner and J. Wolfrum, "How many photons are necessary for fluorescence-lifetime measurements?," Chem. Phys. Lett. **200**, 199–204 (1992).

[29] J. Arlt, D. Tyndall, B. R. Rae, D. D.-U. Li, J. A. Richardson, and R. K. Henderson, "A study of pile-up in integrated time-correlated single photon counting systems," Rev. Sci. Instrum. **84**, 103105 (2013).

[30] A. Bovolenta, A. Cominelli, G. Acconcia, and I. Rech, "Quantifying distortion in time-correlated single photon counting: A universal parameter," Opt. Lett. **49**, 1563–1566 (2024).

[31] P. Peronio, G. Acconcia, I. Rech, and M. Ghioni, "Improving the counting efficiency in time-correlated single photon counting experiments by dead-time optimization," Rev. Sci. Instrum. **86**, 113101 (2015).

[32] S. Tancock, E. Arabul, and N. Dahnoun, "A review of new time-to-digital conversion techniques," IEEE Trans. Instrum. Meas. **68**, 3406–3417 (2019).

[33] R. Machado, J. Cabral, and F. S. Alves, "Recent developments and challenges in FPGA-based time-to-digital converters," IEEE Trans. Instrum. Meas. **68**, 4205–4221 (2019).

[34] C. Niclass and M. Soga, "A miniature actively recharged single-photon detector free of afterpulsing effects with 6 ns dead time in a 0.18 μm CMOS technology," in *2010 International Electron Devices Meeting* (IEEE, 2010), pp. 14–23.

[35] A. Giudici, G. Acconcia, I. Labanca, M. Ghioni, and I. Rech, "4 ns dead time with a fully integrated active quenching circuit driving a custom single photon avalanche diode," Rev. Sci. Instrum. **93**, 043103 (2022).

[36] F. Malanga, G. Fratta, G. Laita, A. Gulinatti, G. Acconcia, and I. Rech, "Double-terminal quenching topology for threefold after-pulsing reduction: Model and experimental validation," IEEE Sens. J. **24**, 28897 (2024).

[37] A. Cuccato, S. Antonioli, M. Crotti, I. Labanca, A. Gulinatti, I. Rech, and M. Ghioni, "Complete and compact 32-channel system for time-correlated single-photon counting measurements," IEEE Photonics J. **5**, 6801514 (2013).

[38] C. Bruschini, H. Homulle, I. M. Antolovic, S. Burri, and E. Charbon, "Single-photon avalanche diode imagers in biophotonics: Review and outlook," Light: Sci. Appl. **8**, 87 (2019).

[39] J. G. Walker, "Iterative correction for 'pile-up' in single-photon lifetime measurement," Opt. Commun. **201**, 271–277 (2002).

[40] M. Patting, P. Reisch, M. Sackrow, R. Dowler, M. Koenig, and M. Wahl, "Fluorescence decay data analysis correcting for detector pulse pile-up at very high count rates," Opt. Eng. **57**, 031305 (2018).

[41] A. Cominelli, G. Acconcia, P. Peronio, M. Ghioni, and I. Rech, "High-speed and low-distortion solution for time-correlated single photon counting measurements: A theoretical analysis," Rev. Sci. Instrum. **88**, 123701 (2017).

[42] F. Malanga, G. Fratta, G. Acconcia, and I. Rech, "Integrated active quenching circuit for high-rate and distortionless spad-based time-resolved fluorescence applications," IEEE Trans. Biomed. Circuits Syst. **19**, 442 (2025).

[43] I. Rech, A. Bovolenta, A. Cominelli, and G. Acconcia, "Toward constraint-less time-correlated single-photon counting measurements: A new method to remove pile-up distortion," IEEE J. Sel. Top. Quantum Electron. **30**, 3800712 (2024).

[44] G. Fratta, P. Daniele, I. Labanca, G. Acconcia, and I. Rech, "Near-zero distortion in TCSPC at more than one photon per excitation period: Experimental validation," Opt. Lett. **49**, 4958–4961 (2024).

[45] W. Hwang, D. Kim, S. Moon, and D. Y. Kim, "Achieving a high photon count rate in digital time-correlated single photon counting using a hybrid photodetector," Opt. Express **29**, 9797–9804 (2021).

[46] J. Meyer, N. J. Gerkau, K. W. Kafitz, M. Patting, F. Jolmes, C. Henneberger, and C. R. Rose, "Rapid fluorescence lifetime imaging reveals that TRPV4 channels promote dysregulation of neuronal Na^+ in ischemia," J. Neurosci. **42**, 552–566 (2022).